IOSR Journal Of Applied Physics (IOSR-JAP)
e-ISSN: 2278-4861.Volume 15, Issue 2 Ser. I (Mar. – Apr. 2023), PP 73-78
www.Iosrjournals.Org

Optimizing the Power Capacity of a Basic Alkaline Battery through Comprehensive Multiphysics Simulation

[1]Venkanna T, [2]Dr. Achal Kiran
[1] Research Scholar of Radha Govind University, Ramgarh (Jharkhand)
[2]Assistant Professor, Radha Govind University, Ramgarh (Jharkhand)

ABSTRACT
Alkaline batteries, especially the primary type, are prevalent in hand-held electronic devices due to their affordability and safety features. The environmental impact caused by their usage and subsequent disposal has led to significant studies focusing on their recyclability. An alternative method to lessen the disposal of these batteries involves enhancing their operational lifespan by improving their energy storage capacity. This study focuses on optimizing the energy capacity of an AA primary alkaline battery. This was achieved by calculating the ideal proportions of electrode materials using advanced multiphysics simulations. A detailed electrochemical model for the alkaline battery was created using the COMSOL Multiphysics software and was tested against real-world data by comparing it with discharge profiles (voltage over time) under fixed resistance conditions. The study aimed to find the optimal electrode thicknesses that would increase the battery's energy capacity without altering its external size. This research also examined how changes in electrode porosity and surface area affect the energy capacity. The developed model successfully mirrored the battery's behavior under a 250 mA steady current discharge. It was observed that reducing the zinc anode's thickness could enhance energy density, but this might lead to anode degradation near the current collectors, potentially disrupting the battery's electrical integrity. Conversely, a thicker anode prevents this degradation but adds to the battery's non-functional mass. The findings from this research could pave the way for producing more durable alkaline batteries. Additionally, the model could be refined by incorporating thermal dynamics or adapted for the development of rechargeable alkaline batteries.
Keywords*: Alkaline Battery Optimization, Multiphysics Simulation, Electrochemical Modeling, Energy Density Enhancement, Electrode Material Analysis*

I. INTRODUCTION

The Zn-MnO_2 primary alkaline battery, commonly found in low-power portable devices like toys, radios, and flashlights, has become a market leader among single-use batteries. Its market is projected to expand by approximately USD 494 million between 2020 and 2024. However, the downside is that about 90% of these batteries are discarded in landfills, primarily due to their single-use design. This situation has sparked interest in both extracting valuable materials from depleted primary alkaline batteries and reengineering the Zn-MnO_2 battery to be rechargeable for large-scale energy storage applications.

A different approach to enhancing the utility of primary alkaline batteries involves improving their energy storage capacity. This can be done by fine-tuning the composition of the materials within the battery. Similar strategies have been applied to other battery types using multiphysics modeling, which involves complex simulations based on the principles of physics and chemistry. These models aim to achieve optimal performance, focusing on factors like energy density. For example, research has been done on lithium-ion batteries to determine the ideal electrode thickness and porosity for maximizing energy and power density.

Multiphysics models are also valuable for analyzing various aspects of battery design, including concentration, temperature, potential, material utilization, and porosity. These insights can guide improvements in battery design. For instance, studies have been conducted on lithium-ion batteries to determine the optimal design for current collector tabs, and on lead-acid batteries to design more efficient current collector grids.

Significant research has been conducted on modeling primary alkaline batteries. Noteworthy studies include those focusing on the movement of zinc ions in zinc anodes and comprehensive multiphysics models of the Zn-MnO_2 primary alkaline battery. There has been industry interest in using multiphysics modeling for battery design, as evidenced by presentations from major corporations. Despite these efforts, optimizing these batteries using multiphysics models is relatively unexplored.

In our research, we aimed to maximize the energy density of an AA primary alkaline battery using multiphysics modeling. We developed a comprehensive model in COMSOL Multiphysics, validated it with experimental data, and examined the battery's internal processes over time. We simulated batteries with varying electrode thicknesses and compared their energy densities, also analyzing how these changes affected the internal workings of the battery. This study underscores the potential of multiphysics modeling in enhancing the

performance of primary alkaline batteries, a frontier not extensively explored in previous research.

II. Methodology

This section initially outlines the observed discharge curves from experimental data, followed by a detailed explanation of the multiphysics model and its application in enhancing the performance of the primary alkaline battery.

2.1 Experimental Data

The study examines voltage versus discharge profiles for an Energizer AA primary alkaline battery, as detailed in the manufacturer's 2018 datasheet. The discharge curve at 250 mA was chosen for analysis due to its relevance to typical battery usage.

2.2 System Description

Figure 1 displays a schematic representation of the primary alkaline battery structure. Central to its operation is a brass anodic current collector, which facilitates electron transfer from the zinc anode during the battery's discharge phase. The chemical reaction at the zinc anode involves the oxidation of zinc in the presence of hydroxide ions (OH^-) from the KOH electrolyte, forming $Zn(OH)4^{2-}$ as depicted in Eq(1). Should there be a low concentration of OH^-, $Zn(OH)4^{2-}$ can transform into ZnO, as indicated in Eq(2). On the other side, the cathode involves MnO2 interacting with water, leading to its reduction to MnOOH and concurrently producing OH^-, as outlined in Eq(3). This cathodic reaction is facilitated by a steel current collector. Separating these components is a separator constructed from polyvinyl alcohol (PVA).

$$Zn(s) + 4OH^-(aq) \rightarrow Zn(OH)^2{}_4{}^-(aq) + 2e^- \quad (1)$$

$$Zn(OH)^2{}_4{}^-(aq) \rightleftharpoons ZnO(s) + H_2O(l) + 2OH^-(aq) \quad (2)$$

$$MnO_2(s) + H_2O(l) + e^- \rightarrow MnOOH(s) + OH^-(aq) \quad (3)$$

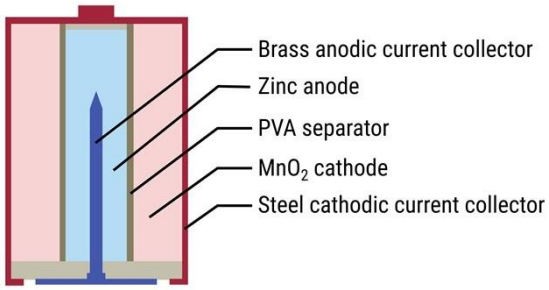

Figure 1: Schematic diagram of a primary alkaline battery.

2.3 Multiphysics model

Figure 2 provides a visual representation of the multiphysics model used for the primary alkaline battery. This model features a one-dimensional axisymmetric framework to depict the mass and charge movement throughout the battery. Additionally, it incorporates distinct particle-scale models for the anode and cathode. The anode is modeled without a specific shape, but its particle-scale model monitors the proportions of zinc and ZnO. Conversely, the cathode is depicted using a core-shell structure, with MnO_2 as the core surrounded by a MnOOH shell. This model also tracks the volume fraction of ZnO that precipitates in the cathode.

Mass and charge transport within the ternary system of K^+, $Zn(OH)4^{2-}$, and OH^- ions are described using Newman's concentrated solution theory. This approach accounts for ion interactions, offering a more comprehensive understanding than the traditional Nernst-Planck equation. The mathematical expressions for mass and charge transport vary across the anode, cathode, and separator, and are elaborated in the work of Podlaha and Cheh (1994). The model adopts Butler-Volmer kinetics for the anode reaction, as explained by Mao and White (1992), while the cathode reaction kinetics are based on the core-shell model by Podlaha and Cheh (1994). The formation of ZnO, a consequence of the surplus of $Zn(OH)4^{2-}$ ions, affects both the anodic and cathodic reactions by reducing the reaction surface area and influencing the mass transfer coefficient for ZnO deposition on the electrodes.

Furthermore, the model takes into account the varying porosities of both electrodes, influenced by the dissolution of zinc, the precipitation of ZnO, and the conversion of MnO_2 into MnOOH. This aspect is crucial for understanding the dynamic changes occurring within the battery during operation.

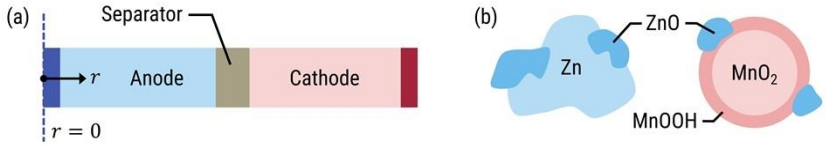

In Figure 2, the battery is conceptualized as a one-dimensional axisymmetric system (a). This representation does not assign a particular particle shape to the zinc anode. Conversely, the MnO_2 cathode is depicted through a core-shell design, with MnOOH forming the shell (b).

2.4 Input Model Parameters

The parameters fed into the multiphysics model are summarized in Table 1. For the cathode, both the reference current density and diffusion coefficient were modified to align with experimental observations, given the lack of specific data for Energizer's primary alkaline batteries. These parameters are also subject to significant variability. The reference current density is influenced by the electrode's surface properties. In contrast, the diffusion coefficient in MnO_2 cathodes shows a broad range of values in existing studies and is affected by the pore structure within the cathode particle.

Table 1: Input parameters to the multiphysics model.

Parameter	Anode	Separator	Cathode
Thickness [cm]	0.361 [a]	0.025 [a]	0.230 [a]
Diffusivity in the solid phase [$cm^2\ s^{-1}$]	N/A	N/A	8.00×10^{-11} [†]
Diffusivity of $K_2Zn(OH)_4$ [$cm^2\ s^{-1}$]	6.00×10^{-6} [b]	6.00×10^{-6} [b]	6.00×10^{-6} [b]
Diffusivity of KOH [$cm^2\ s^{-1}$]	2.19×10^{-5} [b]	2.19×10^{-5} [b]	2.19×10^{-5} [b]
Transport number of $K_2Zn(OH)_4$	0.04 [c]	0.04 [c]	0.04 [c]
Transport number of KOH	0.74 [c]	0.74 [c]	0.74 [c]
Electrical conductivity of the solid phase [S cm^{-1}]	1.83×10^{5} (Zn) [c] 0.01 (ZnO) [c]	0.00 (PVA) 0.01 (ZnO) [c]	19.8 (MnX) [c] 0.01 (ZnO) [c]
Electrical conductivity of the liquid phase [S cm^{-1}]	Correlation in [c]	Correlation in [c]	Correlation in [c]
Reference current density [A cm^{-2}]	0.03 [b]	N/A	1.00×10^{-5} [†]
Mass transfer coefficient of ZnO [cm s^{-1}]	0.005 [c]	0.005 [c]	0.005 [c]
Mass transfer coefficient of $K_2Zn(OH)_4$ [cm s^{-1}]	0.001 [c]	0.001 [c]	0.001 [c]
Initial concentration of $Zn(OH)_4^{2-}$ [mol cm^{-3}]	5.34×10^{-4} [c]	5.34×10^{-4} [c]	5.34×10^{-4} [c]
Initial concentration of OH^- [mol cm^{-3}]	0.007 [c]	0.007 [c]	0.007 [c]
Initial volume fraction of the solid phase	0.26 (Zn) [c] 0.00 (ZnO)	0.20 (PVA) [c] 0.00 (ZnO)	0.76 (MnX) [c] 0.00 (ZnO)
Initial volume fraction of the liquid phase	0.74 [c]	0.80 [c]	0.24 [c]
Initial volumetric surface area [cm^{-1}]	50 [c]	10 [*]	760 [a]
Equilibrium potential [V]	0	N/A	Correlation in [c]
Equilibrium constant for ZnO dissolution	Correlation in [c]	Correlation in [c]	Correlation in [c]

[*] Assumed [†] Fitted to experiment [a] (Chadderdon and Wendling, 2019) [b] (Mao and White, 1992) [c] (Podlaha and Cheh, 1994)

2.5 Case studies

In the initial setup, the primary alkaline battery's performance was simulated using a 250 mA constant discharge current. The model's accuracy was assessed by comparing the predicted voltage versus time curve against actual experimental data. Furthermore, the model generated porosity and concentration profiles within the battery to observe internal changes during discharge.

The optimization process involved simulating the battery under the same 250 mA discharge current but with varying anode thicknesses ranging from 1 cm to 5 cm, and a cutoff voltage of 0.8 V. For each anode thickness, the battery's energy capacity was determined using Eq(4). The anode thickness that yielded the highest energy content was identified as the ideal choice. Throughout this process, the thickness of the separator was kept constant. In contrast, the thicknesses of the cathode were adjusted to maintain the overall battery thickness consistent with the base scenario. Additionally, the porosity and concentration profiles for these varying battery models were analyzed to understand how changes in electrode thickness might affect the battery's operational dynamics.

$$E = \int_0^{tdc} I(t)\, dt \qquad (4)$$

III. RESULTS AND DISCUSSION

3.1 Experimental validation

Figure 3 illustrates a comparative analysis of the voltage versus time data obtained from both simulation and experimentation. The discharge profile generated by the model aligns with the experimental data in its overall pattern, yet it tends to predict a slightly higher voltage. This overestimation of voltage is addressed in the work of Zhang and Cheh (2004), who link it to the difference between the theoretical (Nernstian) and actual electric potentials experienced by the MnO_2 cathode during discharge. Additionally, research conducted by Kozawa and Powers in 1966 provides another perspective, suggesting that the discrepancy might result from the formation of Mn_2O_3, rather than MnOOH, in the later stages of discharge. The energy densities derived from the experimental and simulated data are 2.86 Wh and 3.00 Wh, respectively. This results in a minor discrepancy of approximately 4.93% in the prediction of energy density by the model.

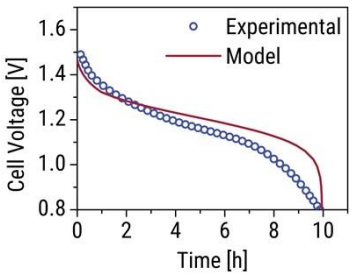

Figure 3: Comparison between experimental and simulated voltage vs. time data.

3.2 Base scenario

Figure 4 displays the evolution of porosity and concentration profiles over time within the battery. These profiles are key to understanding how the compositions of the solid phases vary during the battery's operation. In the anode and separator, a decrease in porosity is observed, which is indicative of a buildup of ZnO. This is due to the fact that ZnO has a larger molar volume compared to zinc. Likewise, a reduction in porosity in the cathode suggests an increased conversion or utilization, as MnOOH possesses a higher molar volume than MnO_2.

The deposition of ZnO at the cathode is minimal because the high concentration of OH^- ions reverts ZnO back into $Zn(OH)4^{2-}$. Near the interface of the anode and separator, zinc anode dissolves into $Zn(OH)4^{2-}$, which subsequently precipitates as ZnO throughout the anode and separator. As a result, the concentration of $Zn(OH)4^{2-}$ is at its highest near this interface and diminishes on the left side of the interface and within the separator.

Regarding the OH^- ions, their concentration increases in the cathode due to their production in the cathodic reaction, while a decrease is noted in the anode due to their consumption in the anodic reaction. Notably, the highest concentration of OH^- in the anode is near the separator, a consequence of OH^- production during the precipitation of $Zn(OH)4^{2-}$. It is also important to mention that the porosity and concentration profiles observed in this study closely align with those reported by Podlaha and Cheh in 1994.

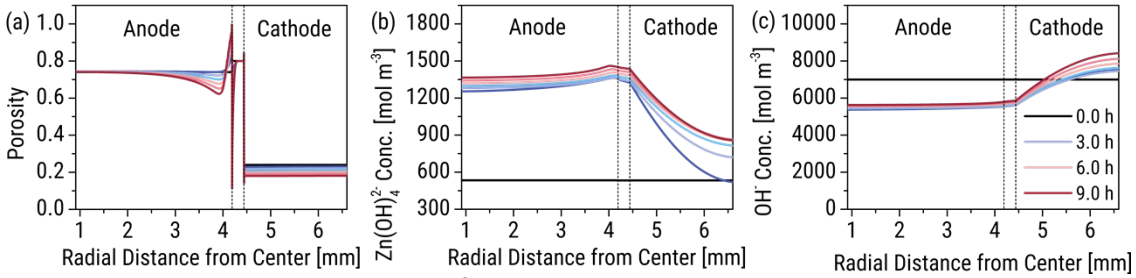

Figure 4: Evolution of the porosity (a), $Zn(OH)_4^{2-}$ concentration (b), and OH^- concentration (c) profiles in the primary alkaline battery over time.

3.3 Optimization scenarios

Figure 5 showcases the energy capacities and discharge characteristics of primary alkaline batteries with differing electrode thicknesses. It was observed that an anode with a thickness of 2 cm delivers the most optimal energy density. In contrast, an anode with a 1 cm thickness was found to be less efficient, as it leads to a premature

cessation of discharge, typically in under 10 hours. Conversely, anodes with a thickness of 3 cm or more are associated with reduced discharge times. This is attributed to the diminished content of the cathode, which accelerates the conversion of MnO_2 to MnOOH.

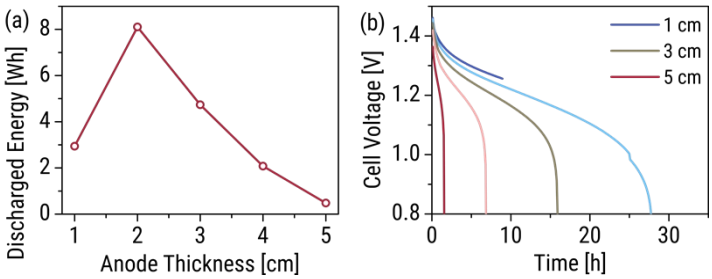

Figure 5: The figure effectively illustrates the comparison between energy capacity (part a) and the voltage versus time curves (part b) for anode thicknesses ranging from 1 cm to 5 cm.

The sudden termination of discharge in the battery with a 1 cm thick anode is elucidated by the porosity profile depicted in Figure 6. The accumulation of ZnO precipitate at the separator effectively halts the ionic current, leading to the end of the discharge process. This phenomenon is particularly evident in the 1 cm anode scenario, where the imbalance between the small anode and larger cathode results in a significant rise in $Zn(OH)4^{2-}$ concentration and a relatively minor decrease in OH^- concentration for each coulomb discharged. The depleted concentration of OH^- ions fails to stabilize $Zn(OH)4^{2-}$, leading to increased precipitation. This mechanism also sheds light on why the minimum porosity rises as the anode thickness increases.

In the case of the battery with a 2 cm thick anode, the porosity profile indicates zinc dissolution not only at the anode-separator interface but also near the interface between the current collector and the anode. This is evidenced by the increase in $Zn(OH)4^{2-}$ concentration and the decrease in OH- concentration near the current collector-anode interface. The augmented dissolution of the anode is attributed to the reduced quantity of zinc compared to the MnO^2 content. Unfortunately, this raises the risk of the zinc anode detaching from the current collector, which would impede current flow to the anode, rendering it ineffective and ultimately ceasing battery operation.

Considering these factors, an anode thickness of 3 cm emerges as a balanced choice between performance and mechanical stability. The porosity profiles suggest that in this scenario, the zinc anode is primarily consumed near the separator without significant dissolution near the current collector. However, further increasing the anode thickness beyond 3 cm leads to a decline in the battery's energy content, as indicated by the accelerated exhaustion of the MnO^2 cathode, as observed in the porosity profiles.

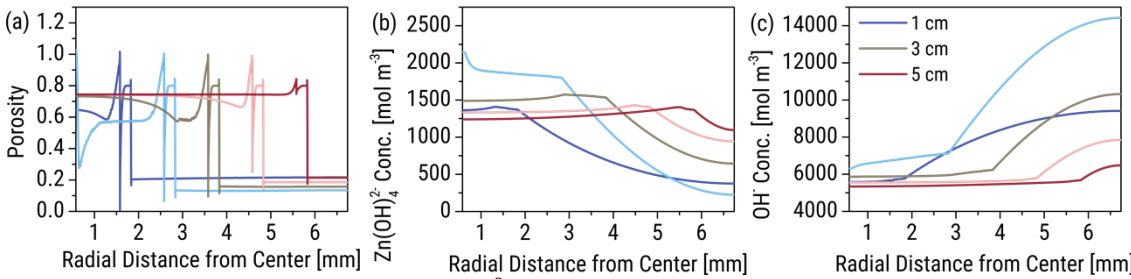

Figure 6: Comparison of the porosity (a), $Zn(OH)_4^{2-}$concentration (b), and OH- concentration (c) profiles at the end of discharge when the anode thicknesses are varied from 1 cm to 5 cm.

IV. Conclusions

This research focused on enhancing the energy capacity of an AA primary alkaline battery through advanced multiphysics simulation. The battery model was developed in COMSOL Multiphysics® and cross-validated against experimental data from Energizer Holdings Inc. Analysis of the porosity and concentration profiles within the battery was crucial to understanding the reactions and ion transport mechanisms. The optimization process involved simulating batteries with different electrode thicknesses, assessing their energy capacities, and observing changes in the reaction and ion transport dynamics.

The simulation successfully mirrored the overall pattern of the experimentally obtained voltage versus time data, although it showed a tendency to estimate voltage on the higher side. The analysis of porosity and concentration profiles indicated that zinc anode consumption predominantly occurs near the anode-separator interface and that ZnO accumulates in both the anode and separator. The optimization results suggested that an anode thickness of 2 cm offers the highest energy capacity for the primary alkaline battery. However, this

configuration leads to zinc dissolution at the interface between the current collector and the anode, potentially affecting the anode's mechanical integrity. Therefore, an anode thickness of 3 cm is advised, as it provides a better balance between energy capacity and structural stability, despite a slight decrease in energy output.

Nomenclature

E – energy capacity, Ah
I – current, A
t – time, h
t_{dc} – discharge time, h
V – voltage, V

References

[1]. Business Wire, 2020, Alkaline battery report – World market to hrow by USD 493.35 million by 2024, Business Wire <https://www.businesswire.com/news/home/20201104005283/en/> accessed 13.03.2022.
[2]. Chadderdon X.H., Wendling M.T., 2019, Mathematical modeling of primary Zn/MnO_2 alkaline batteries, COMSOL <https://www.comsol.com/paper/mathematical-modeling-of-primary-zn-mno2-alkaline-batteries80991> accessed 13.03.2022.
[3]. Edison T.N.J.I., Atchudan R., Karthik N., Xiong D., Lee Y.R., 2019, Direct electro-synthesis of MnO_2 nanoparticles over nickel foam from spent alkaline battery cathode and its supercapacitor performance, Journal of the Taiwan Institute of Chemical Engineers, 97, 414–423.
[4]. Energizer, 2018, Product datasheet Energizer E91, Enegizer <http://data.energizer.com/PDFs/E91.pdf> accessed 13.03.2022
[5]. Farrell T.W., Please C.P., 2005, Primary alkaline battery cathodes, Journal of The Electrochemical Society, 152, A1930.
[6]. Kozawa A., Powers R., 1966, The manganese dioxide electrode in alkaline electrolyte: The electron-proton mechanism for the discharge process from MnO_2 to $MnO_{1.5}$, Journal of The Electrochemical Society, 113, 870–878.
[7]. Seo J.K., Shin J., Chung H., Meng P.Y., Wang X., Meng Y. S., 2018, Intercalation and conversion reactions of nanosized β-MnO_2 cathode in the secondary Zn/MnO_2 alkaline battery, Journal of Physical Chemistry C, 122, 11177–11185.
[8]. Sunu W.G., Bennion, D.N., 1980, Transient and failure analyses of the porous zinc electrode: II. Experimental, Journal of The Electrochemical Society, 127, 2017–2025.